Supporting Information: Balancing DFT Interaction Energies in Charged Dimers Precursors to Organic Semiconductors

Alberto Fabrizio,[†,‡] Riccardo Petraglia,[†] and Clemence Corminboeuf[*,†,‡]

†*Laboratory for Computational Molecular Design, Institute of Chemical Sciences and Engineering, École Polytechnique Fédérale de Lausanne, 1015 Lausanne, Switzerland*

‡*National Centre for Computational Design and Discovery of Novel Materials (MARVEL), École Polytechnique Fédérale de Lausanne, 1015 Lausanne, Switzerland*

E-mail: clemence.corminboeuf@epfl.ch

1 the CryOrel Set

A dataset containing all relevant structural and benchmark data is available Materials Cloud public repository, DOI:10.24435/materialscloud:2020.0012/v1.

Table S1: Abbreviations used in the CryOrel set

	Abbreviation	Definition	CSD Ref. Code
Type I			
	DITT:	(diindeno)-dithienothiophene	SUJLAL
	ETTDM-TTF:	(ethylenethio)(thiodimethylene)--tetrathiafulvalene	Original Paper[S1]
	FPP-DTT:	(perfluorophenyl)(phenyl)--dithienothiophene	DONBUF
Type II			
	BBBT:	benzo-bis(benzothiophene)	SIRMIQ
	BDT:	bis(dithiophene)	Original Paper[S2]
	DBT-Sulfone:	dibenzothiophene-Sulfone	DBTHPS01
Type III			
	BTTT:	bis(thiophene)-thienothiophene	QEPLIH
	DBT:	dibenzothiophene	DBZTHP01
	QTH:	quaterthiophene	PEWXAQ

2 ωB97X-dDsC

Equations 1, 2 and 3 illustrate the general form of the GGA exchange-correlation core, which is characteristic of the B97 family.[S3]

$$E_X^{GGA} = \sum_\sigma \int d\boldsymbol{r} \cdot e_{X\sigma}^{LSDA}(\rho_\sigma) \sum_{i=0}^{m} C_{X,i} u^i \tag{1}$$

$$E_{C\sigma\sigma}^{GGA} = \int d\boldsymbol{r} \cdot e_{C\sigma\sigma}^{LSDA}(\rho_{\sigma\sigma}) \sum_{i=0}^{m} C_{C\sigma\sigma,i} u^i \tag{2}$$

$$E_{C\alpha\beta}^{GGA} = \int d\boldsymbol{r} \cdot e_{C\alpha\beta}^{LSDA}(\rho_{\alpha\beta}) \sum_{i=0}^{m} C_{C\alpha\beta,i} u^i \tag{3}$$

where e_X^{LSDA} is the LSDA exchange factor, $e_{C\sigma\sigma}^{LSDA}$ the same-spin correlation factor, $e_{C\alpha\beta}^{LSDA}$ the opposite-spin correlation factor. The corresponding polynomial expansion coefficients

are indicated with a capital C. u^i is a function of the reduced density gradient (s) weighted by an attenuation factor (γ) and it has the following general form:

$$u = \frac{\gamma s^2}{1 + \gamma s^2}. \tag{4}$$

In ωB97X-dDsC, as in ωB97X-D,[S4] the polynomial expansion in Equations 1, 2 and 3 is truncated at the fourth power (m=4). Building upon the GGA form, the exchange contribution of the range-separated hybrid functional is constructed as follows:

$$E_X = \sum_\sigma \int d\boldsymbol{r} \cdot e_{X\sigma}^{LSDA-SR(\omega)}(\rho_\sigma) \sum_{i=0}^{m} C_{X,i} u^i + C_X^{HF} \cdot E_X^{HF-SR(\omega)} + E_X^{HF-LR(\omega)} \tag{5}$$

where C_X^{HF} is the parameter determining the fraction of exact (Hartree-Fock) exchange at short range.

Adding the contribution from the dDsC dispersion correction[S5–S7] to Equations 2, 3 and 5 yields the full exchange-correlation ωB97X-dDsC functional:

$$E_{XC}^{\omega B97X-dDsC} = E_X + E_{C\sigma\sigma}^{GGA} + E_{C\alpha\beta}^{GGA} + E_{dDsC} \tag{6}$$

Each component of Equation 6 is tuned by at least two adjustable parameters. Table S2 resumes the numerical value of all the optimized coefficients for ωB97X-dDsC, ωB97X+dDsC (where only the dispersion correction is reparametrized), ωB97X-D and ωB97X-D3. The latter functionals are included for comparison purposes.

Table S2: Adjustable parameters of the ωB97X-D, ωB97X-D3, ωB97X-dDsC and ωB97X+dDsC functionals

	-D	-D3	-dDsC	+dDsC
C_x^{HF}	0.222036	0.195728	0.202143	0.157706
C_x^0	0.777964	0.804272	0.797857	0.842294
C_x^1	0.661160	0.698900	-0.100588	0.726479
C_x^2	0.574541	0.508940	2.371856	1.04760
C_x^3	-5.25671	-3.744903	-0.099302	-5.70635
C_x^4	11.6386	10.060790	1.647653	1.32794
$C_{c,\sigma\sigma}^0$	1.000000	1.000000	1.000000	1.000000
$C_{c,\sigma\sigma}^1$	-6.90539	2.433266	-5.161406	-4.33879
$C_{c,\sigma\sigma}^2$	31.3343	-15.446008	21.971045	18.2308
$C_{c,\sigma\sigma}^3$	-51.0533	17.644390	-36.945577	-31.7430
$C_{c,\sigma\sigma}^4$	26.4423	-8.879494	20.00011	17.2901
$C_{c,\alpha\beta}^0$	1.000000	1.000000	1.000000	1.000000
$C_{c,\alpha\beta}^1$	1.794130	-4.868902	5.479632	2.37031
$C_{c,\alpha\beta}^2$	-12.047700	21.295726	-28.015938	-11.3995
$C_{c,\alpha\beta}^3$	14.084700	-36.020866	19.533086	-31.7430
$C_{c,\alpha\beta}^4$	-8.50809	19.177018	3.351842	17.2901
ω	0.200000	0.25	0.275752	0.3
a	6	-	-	-
$s_{r,6}$	-	1.281	-	-
$s_{r,8}$	-	1.094	-	-
ATT0	-	-	59.57	23.30
BTT0	-	-	1.25	0.757

3 Optimization Algorithm

Figure S1 is a diagrammatic illustration of the sequential procedure used in the determination of the 19 adjustable parameters that tune ωB97x-dDsC.

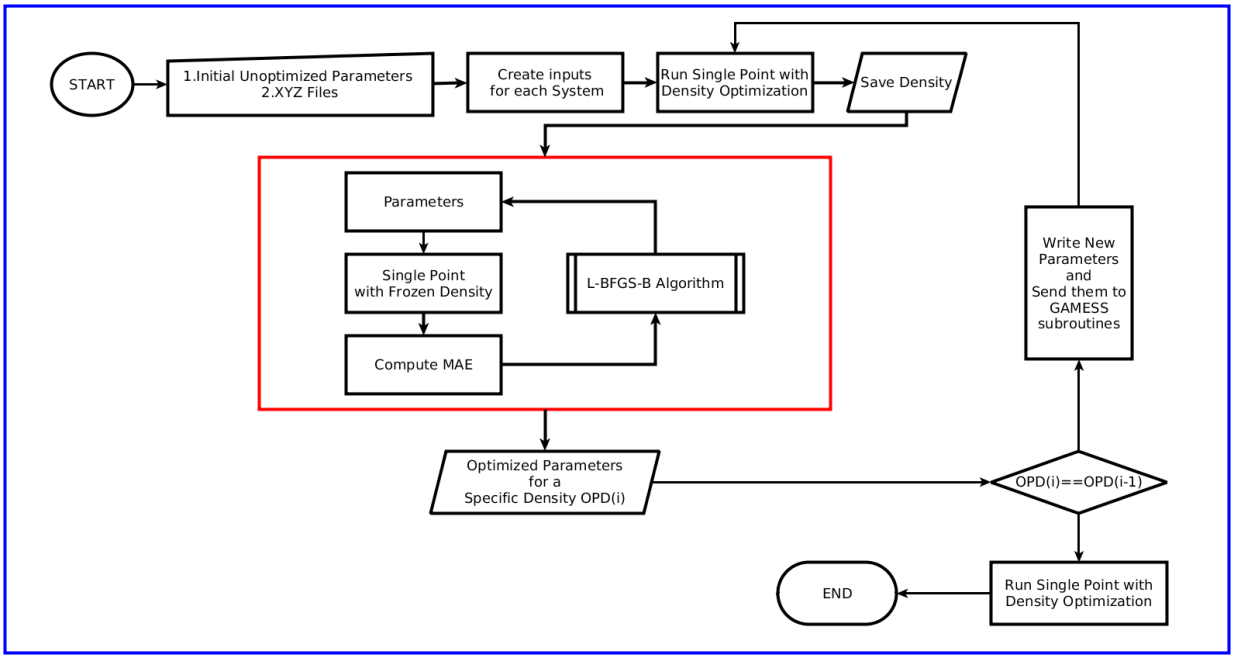

Figure S1: Main algorithm used for the optimization.

The main optimization algorithm is divided in two recursive procedures, delimited in Figure S1 by a blue and a red box. The first one (in blue) is responsible for data generation and storage, input handling and decision making, while the nested processes (in red) perform the actual optimization.

The algorithm requires the user to input the molecular geometry of each molecule of training set (xyz format), as well as to provide the initial guess for the parameters to optimize. Those data are used to generate input files compatible with a modified version of the GAMESS program package[S8,S9] and then to run a single point computation where the electronic densities are optimized self-consistently. The relaxed densities and the effective atomic polarizabilities are then stored as external files in the memory (RAM). Using the data stored in the RAM, the core optimization process computes single point energies and returns

the mean absolute error (MAE) of the training set relative to a specific array of parameters. The MAE is then minimized using a constrained version of the Broyden-Fletcher-Goldfarb-Shanno algorithm (L-BFGS-B),[S10] in order to find the optimal parameters for a specific density (OPD(i)). At this point, the algorithm is able to compare the initial and the updated parameters and decide to either conclude the optimization or to iterate the cycle. The convergence criterion is met when the array of parameters remain unchanged after the optimization process.

The orginal GAMESS code was adapted to the necessity of reading functional parameters from an external input and storing important data, densities and polarizabilities in external unformatted files. A renewed version of the subroutines for the computation of the dDsC dispersion correction was also implemented in the final operational version. The optimization core was designed to use only 14 subroutines of the entire GAMESS program package in order to return the single point energy for each chemical system.

4 Basis Set Dependence

The training and the validation of ωB97X-dDsC has been performed using Ahlrichs def2-TZVPD basis set. Here, we compare the performance of the functional on the Orel26rad set in combination with the def2-TZVPD, def2-TZVP and the much smaller 6-31G* basis sets (Figure S2).

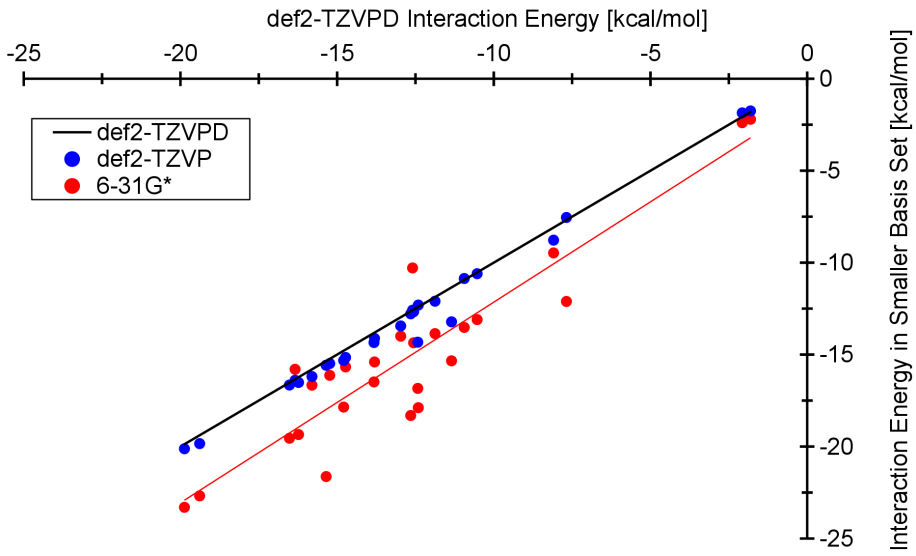

Figure S2: Correlation between the interaction energies of Orel26rad, computed with def2-TZVPD (reference), def2-TZVP and 6-31G*.

The interaction energies of the computed with ωB97X-dDsC are robust with respect to different basis sets. Giving up the computationally expensive diffuse functions does not influence in any way the results. Even using a much smaller basis (6-31G*), the results deviate only slightly from the reference. Therefore, the influence of the basis set choice is only marginal and highly accurate result can be obtained already with def2-TZVP.

5 Functional parametrization and Validation

Table S3: Values of the mean absolute error (MAE) in kcal mol^{-1} of ωB97X-D and ωB97X-dDsC on the training set

	ωB97X-D	ωB97X-dDsC
All	1.98	1.79
G2-148	2.48	2.13
IP-36	2.70	2.66
EA-25	2.36	2.71
PA-8	1.71	1.01
HTBH-38	2.64	1.88
NHTBH-38	1.57	1.69
S-22	0.40	0.44

Table S4: Values of the mean absolute error (MAE) in kcal mol^{-1} of illustrative functionals on Orel26rad and Pi29n.

	Orel26rad	Pi29n
ωB97X-dDsC	0.998	0.508
ωB97M(2)	1.033	0.327
ωB97X-D	1.410	0.410
ωB97X-D3	1.704	0.229
ωB97X-V	2.255	0.169
ωB97X+dDsC	2.482	0.262
ωB97M-V	2.605	0.113
ωM06-D3	2.840	0.180
ωB97X	3.693	1.513
LC-BOP-LRD	2.847	0.303
PBE0-dDsC	7.520	0.510

Table S5: Furan profile: values in kcal mol^{-1}.

C.O.M distance [Å]	CCSD(T)/CBS	PBE0-dDsC	LC-BOP-LRD	ωB97X-dDsC
2.6	-14.285	-17.518	-9.254	-10.954
2.7	-17.893	-21.473	-13.506	-15.689
2.8	-19.722	-23.801	-15.866	-18.511
2.9	-20.3	-24.836	-16.858	-19.872
3	-20.018	-25.016	-16.898	-20.148
3.1	-19.192	-24.625	-16.315	-19.725
3.2	-18.026	-23.938	-15.355	-18.839
3.3	-16.685	-23.02	-14.202	-17.694
3.4	-15.263	-22.019	-12.984	-16.325
3.5	-13.852	-21.018	-11.782	-14.958
3.6	-12.495	-20.023	-10.646	-13.565
4.1	-7.286	-16.132	-6.423	-7.997
4.6	-4.566	-14.054	-4.156	-4.91
5.1	-3.165	-13.147	-2.924	-3.334
5.6	-2.337	-12.972	-2.21	-2.435
6.1	-1.804	-12.972	-1.727	-1.865
6.6	-1.425	-13.055	-1.379	-1.467

Table S6: Thiophene profile: values in kcal mol^{-1}.

C.O.M distance [Å]	CCSD(T)/CBS	PBE0-dDsC	LC-BOP-LRD	ωB97X-dDsC
2.9	-8.485	-10.46	-1.884	-4.267
3	-11.598	-14.079	-5.901	-8.532
3.1	-13.369	-16.38	-8.432	-11.196
3.2	-14.153	-17.643	-9.893	-12.652
3.3	-14.264	-18.226	-10.607	-13.325
3.4	-13.913	-18.282	-10.799	-13.344
3.5	-13.28	-18.064	-10.633	-12.955
3.6	-12.47	-17.611	-10.237	-12.294
3.7	-11.592	-17.071	-9.713	-11.513
3.8	-10.698	-16.509	-9.121	-10.674
3.9	-9.828	-15.895	-8.498	-9.811
4.4	-6.39	-13.323	-5.704	-6.32
4.9	-4.383	-11.853	-3.907	-4.346
5.4	-3.181	-11.204	-2.868	-3.188
5.9	-2.414	-11.1	-2.236	-2.439
6.4	-1.883	-11.164	-1.739	-1.913
6.9	-1.509	-11.333	-1.444	-1.526

The performance of ωB97X-dDsC has been analysed on 7 subsets of the GMTKN30 database in addition to the 7 reported for the training of the functional (G2, IP, EA, PA, HTBT, NHTH, S22), as well as Orel26rad and Pi29n. In particular, we tested the accuracy of ωB97X-dDsC on the relative energies of the conformers in alkanes, cysteine, sugars and PGG tripeptides (ACONF,[S11] CYCONF,[S12] SCONF,[S13] PCONF[S14]), the interaction energies of linear alkane dimers (ADIM6),[S15] the isomerization energies of medium-sized organic molecules (ISO34),[S16] and reaction energies from the G2/97 database (G2RC).[S17] The reference data and geometries of the mentioned datasets have been taken from the original GMTKN30 publication,[S15] although it must be mentioned that the benchmarks for some of these sets has been improved in the more recent GMTKN55 database.[S18] Overall, the performance on these datasets of ωB97X-dDsC/def2-TZVP resembles closely to the values of ωB97X-D/def2-QZVP reported in the literature, despite the difference in the basis set.

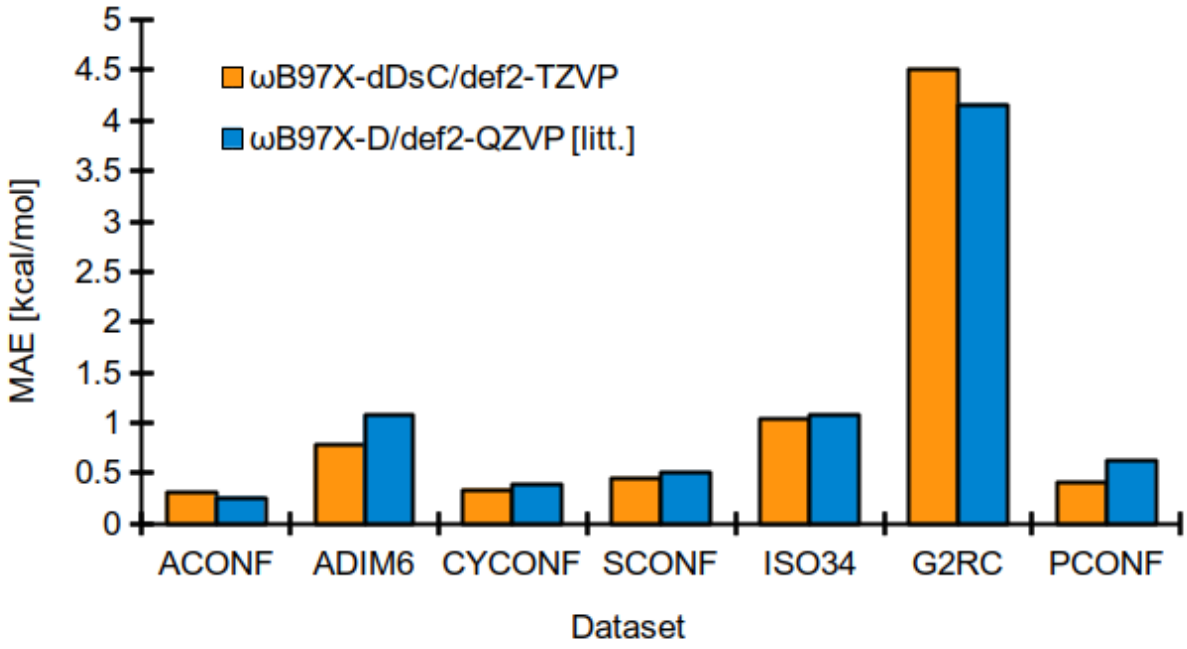

Figure S3: MAE of ωB97X-dDsC/def2-TZVP on 7 subsets of the GMTKN30 database.[S15] ωB97X-D/def2-QZVP values taken from Ref. S15 are reported for comparison.

Table S7: Additinal Validation: MAE values in kcal mol^{-1}.

Dataset	ωB97X-dDsC/ def2-TZVP	ωB97X-D/ def2-QZVP [from Ref. S15]
ACONF	0.31	0.26
ADIM6	0.77	1.07
CYCONF	0.34	0.38
SCONF	0.45	0.51
ISO34	1.04	1.08
G2RC	4.51	4.16
PCONF	0.41	0.62

6 Functional performance on CryOrel.

As visible in Figure S4, the robustness of the theoretical method employed for describing the radical cationic dimers is dictated by its ability to treat delocalization error and London dispersion interactions. These two aspects have been tested using an illustra-

tive set of GGA (B97,[S3] PBE[S19,S20] and BLYP[S21,S22]), meta-GGA (TPSS,[S23] M06L[S24] and M11L[S25]), global hybrid (B3LYP,[S22,S26,S27] PBE0[S28,S29] and BHHLYP[S22,S30]), meta-hybrid (M06,[S31] M06-2X[S31] and M06-HF[S32]) and range-separated hybrid (ωB97X-D,[S4] ωB97X-D3,[S33] ωB97X-V,[S34] ωB97M-V,[S35] ωM06-D3,[S33] M11,[S36] ωB97X-dDsC and ωB97X+dDsC) functionals. Long-range dispersion interactions were accounted for using *ad hoc* post-SCF dispersion corrections (-D3(BJ)[S37] and -dDsC[S5–S7]), as well as nonlocal correlation functionals (*i.e.*, VV10,[S38] for ωB97X-V, ωB97M-V) or effective one-electron potentials (M06 family).

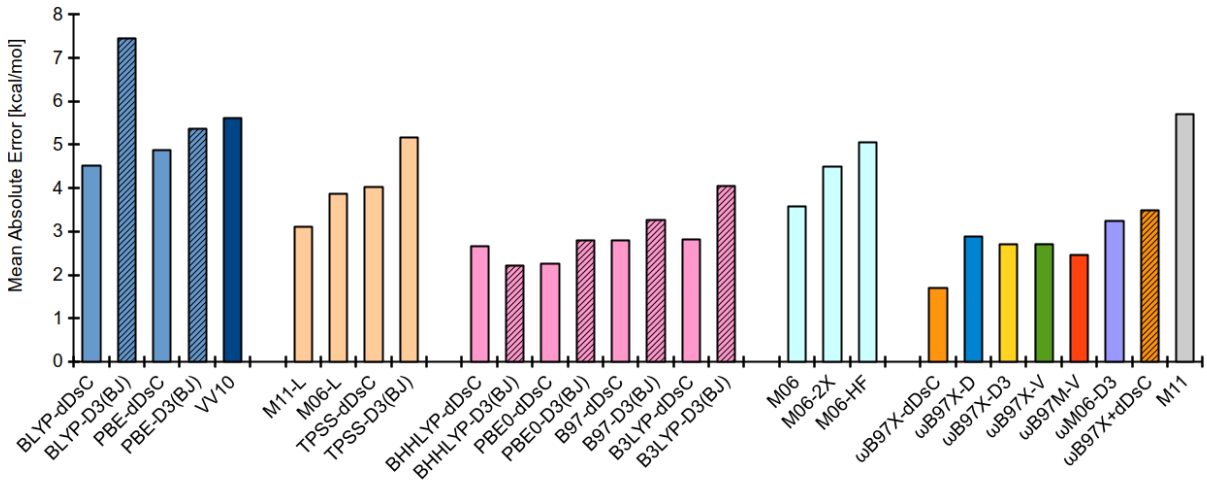

Figure S4: MAE of tested functionals on the CryOrel dataset. Blue: GGAs; pale orange: meta-GGAs; pink: global hybrids; cyan: meta-hybrids. Range-separated hybrids follow the same color code as in previous Figures. Oblique bars are drawn to mark the same functional used with a different dispersion correction.

Table S8: Absolute errors (AE) in kcal $\cdot$ mol^{-1} of the functionals on CryOrel.

Brickwork	DITT	ETTDM-TTF	FPP-DTT
B97-dDsC	4.216	0.838	0.840
B97-D3(BJ)	8.766	1.189	4.196
BLYP-dDsC	5.175	4.091	0.508
BLYP-D3(BJ)	1.536	11.001	6.175
PBE-dDsC	4.279	4.492	1.175
PBE-D3(BJ)	6.109	5.947	0.415
VV10	3.302	6.788	2.514

Table S8: Absolute errors (AE) in kcalmol^{-1} of the functionals on CryOrel (continue).

M11-L	10.771	2.43	7.888
M06-L	10.819	2.172	4.952
TPSS-dDsC	4.654	3.761	0.459
TPSS-D3(BJ)	3.826	7.559	1.503
BHHLYP-dDsC	5.333	3.411	3.442
BHHLYP-D3(BJ)	7.242	0.343	4.324
PBE0-dDsC	3.638	0.95	0.084
PBE0-D3(BJ)	6.096	2.546	1.713
B3LYP-dDsC	2.701	1.883	0.371
B3LYP-D3(BJ)	2.14	6.02	2.17
M06	11.27	0.885	7.623
M06-2X	9.291	2.89	6.567
M06-HF	14.132	2.218	4.813
ωB97X-dDsC	2.533	1.782	1.702
ωB97X-D	5.642	4.085	4.042
ωB97X-D3	6.585	2.306	5.723
ωB97X-V	5.979	1.732	4.259
ωB97M-V	4.539	0.578	2.559
ωM06-D3	6.679	1.877	5.444
ωB97X+dDsC	9.182	3.689	7.000
M11	12.888	3.105	7.541

Lamellar/Columnar	BBBT	BDT	DBT-Sulfone
B97-dDsC	8.178	0.255	4.068
B97-D3(BJ)	7.215	0.055	2.274
BLYP-dDsC	11.776	1.999	4.929
BLYP-D3(BJ)	11.358	6.434	7.973
PBE-dDsC	10.364	2.929	6.196
PBE-D3(BJ)	10.721	3.946	5.154
VV10	10.717	5.082	5.777
M11-L	1.317	0.751	0.238
M06-L	7.774	3.701	1.593
TPSS-dDsC	9.733	2.888	5.118
TPSS-D3(BJ)	10.35	1.004	5.659
BHHLYP-dDsC	1.197	1.604	0.084
BHHLYP-D3(BJ)	0.690	0.658	0.930
PBE0-dDsC	6.943	0.312	3.519

Table S8: Absolute errors (AE) in kcalmol^{-1} of the functionals on CryOrel (continue).

PBE0-D3(BJ)	6.186	0.767	2.479
B3LYP-dDsC	8.156	0.158	4.046
B3LYP-D3(BJ)	7.576	2.818	4.552
M06	4.046	3.115	0.873
M06-2X	2.735	3.072	2.25
M06-HF	3.813	3.683	3.113
ωB97X-dDsC	0.551	1.202	0.253
ωB97X-D	0.469	2.974	0.354
ωB97X-D3	0.263	1.335	1.396
ωB97X-V	0.875	0.87	2.485
ωB97M-V	0.459	0.321	6.084
ωM06-D3	0.048	0.264	6.833
ωB97X+dDsC	0.073	0.536	2.496
M11	3.056	4.463	3.998
Herringbone	BTTT	DBT	QTH
B97-dDsC	0.241	3.075	3.411
B97-D3(BJ)	2.058	1.530	2.053
BLYP-dDsC	0.042	6.826	5.355
BLYP-D3(BJ)	8.947	6.054	7.652
PBE-dDsC	3.308	5.263	5.806
PBE-D3(BJ)	5.834	4.906	5.276
VV10	6.247	4.726	5.315
M11-L	2.022	1.275	1.376
M06-L	1.381	1.604	0.795
TPSS-dDsC	0.366	4.874	4.428
TPSS-D3(BJ)	6.39	4.711	5.512
BHHLYP-dDsC	5.522	1.240	2.128
BHHLYP-D3(BJ)	1.337	2.200	2.300
PBE0-dDsC	0.245	2.159	2.443
PBE0-D3(BJ)	2.360	0.998	1.937
B3LYP-dDsC	1.047	3.283	3.621
B3LYP-D3(BJ)	4.817	2.441	3.941
M06	1.309	1.149	2.004
M06-2X	4.443	3.845	5.298
M06-HF	4.185	3.578	6.022

Table S8: Absolute errors (AE) in kcalmol^{-1} of the functionals on CryOrel (continue).

ωB97X-dDsC	3.424	1.923	1.929
ωB97X-D	3.250	2.101	3.024
ωB97X-D3	1.805	2.891	2.103
ωB97X-V	2.125	3.237	2.878
ωB97M-V	1.391	3.586	2.61
ωM06-D3	2.076	3.249	2.807
ωB97X+dDsC	2.853	2.795	2.701
M11	5.42	4.504	6.295

All	MAE	MSE	STDEV
B97-dDsC	2.791	-1.557	2.443
B97-D3(BJ)	3.26	-0.379	2.754
BLYP-dDsC	4.522	-3.25	3.366
BLYP-D3(BJ)	7.459	-7.459	2.789
PBE-dDsC	4.868	-3.917	2.434
PBE-D3(BJ)	5.368	-3.918	2.507
VV10	5.608	-4.874	2.210
M11-L	3.119	1.373	3.441
M06-L	3.866	0.461	3.225
TPSS-dDsC	4.031	-2.355	2.636
TPSS-D3(BJ)	5.168	-4.318	2.732
BHHLYP-dDsC	2.662	2.396	1.786
BHHLYP-D3(BJ)	2.225	1.925	2.119
PBE0-dDsC	2.255	-1.323	2.102
PBE0-D3(BJ)	2.787	-1.051	1.885
B3LYP-dDsC	2.807	-1.939	2.308
B3LYP-D3(BJ)	4.053	-3.577	1.778
M06	3.586	2.687	3.4
M06-2X	4.488	2.423	2.137
M06-HF	5.062	1.921	3.359
ωB97X-dDsC	1.700	1.644	0.909
ωB97X-D	2.882	2.882	1.613
ωB97X-D3	2.712	2.712	1.974
ωB97X-V	2.715	2.715	1.545
ωB97M-V	2.459	2.459	1.886
ωM06-D3	3.253	3.253	2.405
ωB97X+dDsC	3.480	3.480	2.742
M11	5.697	2.833	2.888

Table S9: Absolute errors in kcal mol^{-1} of wavefunction-based methods on CryOrel.

Brickwork	DITT	ETTDM-TTF	FPP-DTT
AE RPA/CBS	0.579	1.154	0.001
AE MP2/6-31G*(0.25)	0.619	1.445	1.172
AE U-SAPT0/jun-cc-pVDZ	2.638	0.153	0.343
Lamellar/Columnar	BBBT	BDT	DBT-Sulfone
AE RPA/CBS	0.294	0.631	1.486
AE MP2/6-31G*(0.25)	0.243	0.833	1.366
AE U-SAPT0/jun-cc-pVDZ	0.893	0.094	1.006
Herringbone	BTTT	DBT	QTH
AE RPA/CBS	0.852	0.471	0.216
AE MP2/6-31G*(0.25)	0.648	1.484	0.829
AE U-SAPT0/jun-cc-pVDZ	2.275	1.315	0.231
All	MAE		
RPA/CBS	0.632		
MP2/6-31G*(0.25)	0.96		
U-SAPT0/jun-cc-pVDZ	0.994		

Table S10: Correlation between U-SAPT0/jun-cc-pVDZ contributions and absolute errors (AE) in kcal mol^{-1} of illustrative functionals on CryOrel.

Brickwork	DITT	ETTDM-TTF	FPP-DTT
Pauli Exchange	32.16	29.08	41.59
Dispersion	-48.63	-25.84	-45.11
AE ωB97X-dDsC	2.53	1.78	1.70
AE ωB97X-D	5.64	4.09	4.04
AE ωB97X-D3	6.59	2.31	5.72
AE ωB97X-V	5.98	1.73	4.26
AE ωB97M-V	4.54	0.58	2.56
AE ωM06-D3	6.68	1.88	5.44
Lamellar/Columnar	BBBT	BDT	DBT-Sulfone
Pauli Exchange	6.26	20.1	16.03
Dispersion	-8.09	-16.74	-21.91
AE ωB97X-dDsC	0.55	1.20	0.25
AE ωB97X-D	0.47	2.97	0.35
AE ωB97X-D3	0.26	1.33	1.4
AE ωB97X-V	0.88	0.87	2.48
AE ωB97M-V	0.46	0.32	6.08
AE ωM06-D3	0.05	0.26	6.83
Herringbone	BTTT	DBT	QTH
Pauli Exchange	19.25	8.94	12.78
Dispersion	-22.29	-12.39	-20.35
AE ωB97X-dDsC	3.42	1.92	1.93
AE ωB97X-D	3.25	2.10	3.02
AE ωB97X-D3	1.8	2.89	2.1
AE ωB97X-V	2.13	3.24	2.88
AE ωB97M-V	1.39	3.59	2.61
AE ωM06-D3	2.08	3.25	2.81

7 Spin Densities

The difference between the α- and the β-spin densities (spin-density) is a readily available probe of the charge (de-)localization in real-space. In Figure S5, we report the spin-densities

of three dimers from the CryOrel9 dataset, the first two being representative of the stacked and tilted class and the third (ETTDM-TTF) showing how structural asymmetry helps restoring the correct attribution of radical cation character. The two functionals chosen (ωB97X-dDsC and ωB97M-V) represent opposite bounds of the error on the interaction energies of the stacked dimers, while ωB97X-V is reported for comparison. In the upper panels of Figure S5, it can be seen how ωB97M-V converges to the incorrect solution, attributing the majority of the spin-density to the neutral monomer. In contrast, both functionals correctly describe the spin-densities of the tilted and the asymmetric dimer.

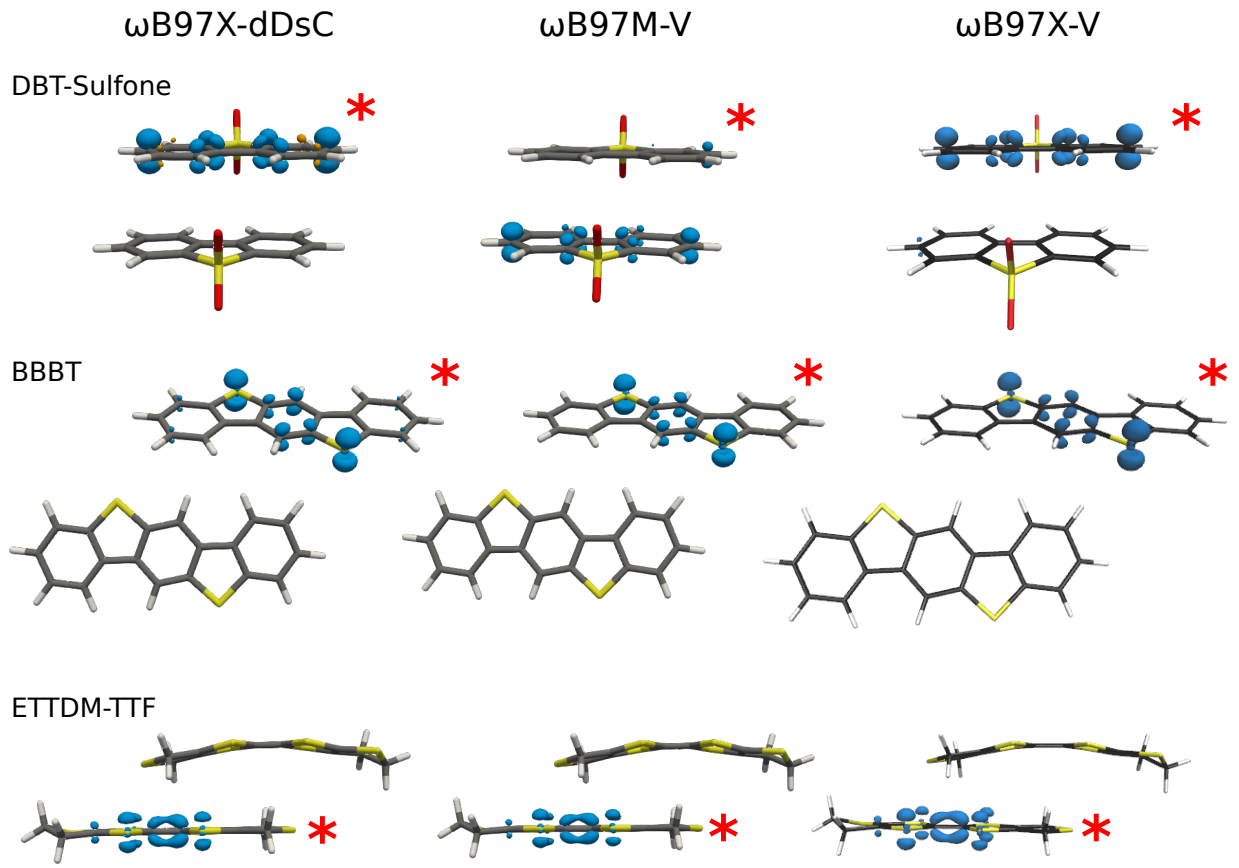

Figure S5: Spin-densities (isovalue: +0.01 $e^{-}Bohr^{-3}$) of DBT-Sulfone (stacked class), BBBT (tilted class) and ETTDM-TTF (stacked, but asymmetric) with two functionals (ωB97X-dDsC and ωB97M-V), representative of the lower and the upper bound of the interaction energy error. ωB97X-V is also reported for comparison. Red asterisks mark which monomer has been optimized as a radical cation.

8 T1 diagnostic of the CryOrel9 dimers at DLPNO-CCSD(T) and BSSE after extrapolation

The reliability of the coupled-cluster computations with respect to possible multireference character of the dimers of the CryOrel9 dataset was analyzed using the common T1-diagnostic.[S39] As shown in the table below, all T1 are smaller than the standard threshold value of 0.02,[S39] indicating the reliability of a single determinant zeroth order reference.

Table S11: T1 diagnostic of the CryOrel9 dimers at DLPNO-CCSD(T)/cc-pVTZ

	Name	T1 diagnostic
Type I		
	DITT:	0.0122
	ETTDM-TTF:	0.0136
	FPP-DTT:	0.0128
Type II		
	BBBT:	0.0135
	BDT:	0.014
	DBT-Sulfone:	0.0146
Type III		
	BTTT:	0.0144
	DBT:	0.0139
	QTH:	0.0141

The table below reports the basis set superposition error (BSSE) for each neutral and the radical monomer in CryOrel9 after extrapolation to estimated CBS at DLPNO-CCSD(T).

Table S12: Basis set superposition error for each neutral and the radical monomer in CryOrel9 after extrapolation to estimated CBS at DLPNO-CCSD(T).

Dimer	BSSE Mon. Neutral [kcal/mol]	BSSE Mon. Radical [kcal/mol]
BBBT	0.217	0.006
BDT	0.305	0.387
BTTT	0.607	0.697
DBT	0.919	0.262
DBT-Sulfone	0.872	0.941
DITT	1.567	1.403
ETTDM-TTF	0.768	0.839
FPP-DTT	2.573	2.305
QTH	0.495	0.708

9 DLPNO-CCSD(T)/cc-pV(D/T)Z on S22, S66 and Orel26rad

The following tables report the performance of DLPNO-CCSD(T) on the interaction energies of three different datasets S22,[S40] S66[S41] and Orel26rad[S42] using the same protocol as applied in this work. Overall, the average performance of the scheme is in good agreement with DLPNO-CCSD(T) results found in the literature [*e.g.* Refs. S43,S44].

Table S13: MAE on S22, S66 and Orel26rad at estimated DLPNO-CCSD(T)/CBS

Dataset	MAE [kcal/mol]
S22	0.45
S66	0.26
Orel26rad	0.58

Table S14: Interaction energies and Absolute Errors of estimated DLPNO-CCSD(T)/CBS on S22

Dimer	Int. Energy [kcal/mol]	Absolute Error [kcal/mol]
1	3.124	0.046
2	4.639	0.381
3	17.781	1.019
4	15.345	0.775
5	19.606	1.084
6	16.459	0.541
7	15.632	1.108
8	0.455	0.075
9	1.429	0.071
10	1.656	0.206
11	3.426	0.806
12	4.813	0.613
13	9.728	0.012
14	5.647	1.057
15	12.266	0.606
16	1.497	0.013
17	3.199	0.091
18	2.378	0.058
19	4.863	0.313
20	3.038	0.328
21	6.057	0.437
22	6.81	0.28

Table S15: Interaction energies and Absolute Errors of estimated DLPNO-CCSD(T)/CBS on Orel26rad

Dimer	Int. Energy [kcal/mol]	Absolute Error [kcal/mol]
1	-16.317	0.353
2	-15.947	0.483
3	-19.015	0.405
4	-11.368	0.462
5	-12.121	0.439
6	-13.415	0.555
7	-15.845	0.775
8	-19.246	1.054
9	-8.792	0.202
10	-2.236	0.346
11	-11.502	0.158
12	-11.324	0.056
13	-13.62	0.12
14	-14.718	0.568
15	-16.775	0.805
16	-12.784	1.676
17	-7.13	1.62
18	-2.42	0.32
19	-14.666	0.436
20	-15.147	0.773
21	-14.804	0.434
22	-15.558	0.032
23	-15.314	0.026
24	-13.04	1.82
25	-17.146	1.144
26	-16.813	0.207

Table S16: Interaction energies and Absolute Errors of estimated DLPNO-CCSD(T)/CBS on S66

Dimer	Int. Energy [kcal/mol]	Absolute Error [kcal/mol]
1	-4.656	0.262
2	-5.19	0.402
3	-6.39	0.518
4	-7.563	0.54
5	-5.338	0.419
6	-7.161	0.393
7	-7.745	0.485
8	-4.723	0.286

9	-2.837	0.222
10	-4.042	0.118
11	-5.294	0.125
12	-6.86	0.406
13	-5.904	0.283
14	-7.216	0.238
15	-8.207	0.423
16	-4.901	0.223
17	-16.27	0.912
18	-6.363	0.494
19	-7.003	0.407
20	-18.24	0.853
21	-15.607	0.658
22	-18.676	0.815
23	-18.461	0.728
24	-3.438	0.616
25	-4.476	0.581
26	-9.711	0.118
27	-4.059	0.62
28	-6.163	0.45
29	-7.18	0.361
30	-1.614	0.182
31	-3.416	0.036
32	-3.737	0.001
33	-2.072	0.2
34	-3.824	0.048
35	-2.515	0.098
36	-1.635	0.142
37	-2.358	0.046
38	-2.964	0.033
39	-3.945	0.37
40	-3.116	0.221
41	-4.9	0.052
42	-4.154	0.016
43	-3.621	0.091
44	-2.026	0.021
45	-1.728	0.02
46	-4.175	0.089
47	-3.122	0.246
48	-3.751	0.216
49	-3.549	0.218
50	-3.141	0.274
51	-1.474	0.05
52	-4.675	0.032

53	-4.261	0.1
54	-3.2	0.077
55	-4.268	0.08
56	-3.407	0.176
57	-5.455	0.173
58	-3.939	0.207
59	-2.862	0.012
60	-4.631	0.237
61	-2.721	0.191
62	-3.33	0.204
63	-3.844	0.043
64	-2.872	0.127
65	-3.966	0.025
66	-3.973	0.005

10 Three body effects and atomic-charge information

Table S17 and Figure S6 report the performance of the PBE0 functional on CryOrel9 in combination with four different dispersion corrections [-dDsC, -D3(BJ), -D3(BJ)-ATM, -D4]. The chosen dispersion corrections allows analyzing the effects of the three-body interactions term (-D3(BJ) vs -D3(BJ)-ATM) and the performance of the latest -D4 correction. Overall, three-body effects do not significantly lower the mean absolute error. Similarly, -D4 does not offer any improvement upon -D3(BJ) or -dDsC.

Table S17: Comparison of the interaction energies and the MAE on CryOrel between different dispersion corrections to the PBE0 functional. The last column refers to the effects of 3-body term on the interaction energies in percentage.

	PBE0-dDsC	PBE0-D3(BJ)	PBE0-D3(BJ)-ATM	PBE0-D4	% ATM Int. Energies
DITT	-36.856	-34.398	-32.983	-37.783	4.115
ETTDM-TTF	-19.418	-21.014	-20.475	-22.254	2.564
FPP-DTT	-27.596	-25.799	-24.665	-28.504	4.395
BBBT	-12.595	-11.837	-11.787	-11.897	0.423
BDT	-12.415	-13.494	-13.395	-14.671	0.739
DBT-Sulfone	-23.159	-22.119	-21.43	-22.929	3.114
BTTT	-12.737	-15.342	-14.891	-16.443	2.937
DBT	-18.387	-17.227	-16.921	-17.468	1.775
QTH	-17.228	-16.722	-16.274	-17.478	2.679
MAE	2.255	2.787	2.783	2.929	

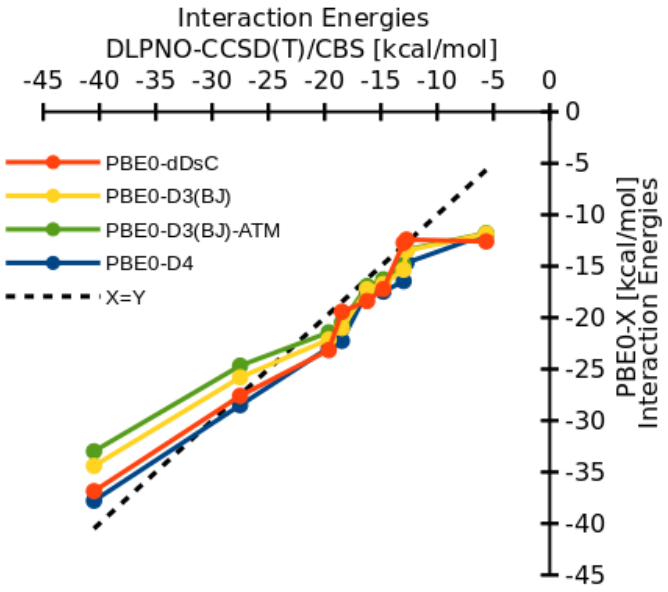

Figure S6: Correlation plot between PBE0/TZVP combined with different dispersion corrections and DLPNO-CCSD(T)/CBS interaction energies for the CryOrel9 dataset.

References

(S1) Mas-Torrent, M.; Hadley, P.; Bromley, S. T.; Ribas, X.; Tarrés, J.; Mas, M.; Molins, E.; Veciana, J.; Rovira, C. Correlation between crystal structure and mobility in organic field-effect transistors based on single crystals of tetrathiafulvalene derivatives. *J. Am. Chem. Soc* **2004**, *126*, 8546–8553.

(S2) Li, X.-C.; Sirringhaus, H.; Garnier, F.; Holmes, A. B.; Moratti, S. C.; Feeder, N.; Clegg, W.; Teat, S. J.; Friend, R. H. A highly π-stacked organic semiconductor for thin-film transistors based on fused thiophenes. *J. Am. Chem. Soc.* **1998**, *120*, 2206–2207.

(S3) Becke, A. D. Density-functional thermochemistry. V. Systematic optimization of exchange-correlation functionals. *J. Chem. Phys.* **1997**, *107*, 8554.

(S4) Chai, J.-D.; Head-Gordon, M. Long-range corrected hybrid density functionals with damped atom-atom dispersion corrections. *Phys. Chem. Chem. Phys.* **2008**, *10*, 6615–6620.

(S5) Steinmann, S. N.; Corminboeuf, C. A System-Dependent Density-Based Dispersion Correction. *J. Chem. Theory Comput.* **2010**, *6*, 1990–2001.

(S6) Steinmann, S. N.; Corminboeuf, C. A generalized-gradient approximation exchange hole model for dispersion coefficients. *J. Chem. Phys.* **2011**, *134*, 44117.

(S7) Steinmann, S. N.; Corminboeuf, C. Comprehensive Benchmarking of a Density-Dependent Dispersion Correction. *J. Chem. Theory Comput.* **2011**, *7*, 3567–3577.

(S8) Schmidt, M. W.; Baldridge, K. K.; Boatz, J. A.; Elbert, S. T.; Gordon, M. S.; Jensen, J. H.; Koseki, S.; Matsunaga, N.; Nguyen, K. A.; Su, S.; Windus, T. L.; Dupuis, M.; Montgomery, J. A. General atomic and molecular electronic structure system. *J. Comput. Chem.* **1993**, *14*, 1347–1363.

(S9) Gordon, M. S.; Schmidt, M. W. In *Theory and Applications of Computational Chemistry*; Dykstra, C., Frenking, G., Kim, K., Scuseria, G., Eds.; Elsevier: Amsterdam, 2005; pp 1167–1189.

(S10) Byrd, R. H.; Lu, P.; Nocedal, J.; Zhu, C. A Limited Memory Algorithm for Bound Constrained Optimization. *SIAM J. Sci. Comput.* **1995**, *16*, 1190–1208.

(S11) Gruzman, D.; Karton, A.; Martin, J. M. L. Performance of Ab Initio and Density Functional Methods for Conformational Equilibria of C_nH_{2n+2} Alkane Isomers (n= 4-8). *J. Phys. Chem. A* **2009**, *113*, 11974–11983.

(S12) Wilke, J. J.; Lind, M. C.; Schaefer, H. F.; Császár, A. G.; Allen, W. D. Conformers of Gaseous Cysteine. *J. Chem. Theory Comput.* **2009**, *5*, 1511–1523.

(S13) Goerigk, L.; Grimme, S. A general database for main group thermochemistry, kinetics, and noncovalent interactions - Assessment of common and reparameterized (meta-) GGA density functionals. *J. Chem. Theory Comput.* **2010**, *6*, 107–126.

(S14) Řeha, D.; Valdés, H.; Vondrášek, J.; Hobza, P.; Abu-Riziq, A.; Crews, B.; de Vries, M. S. Structure and IR Spectrum of Phenylalanyl-Glycyl-Glycine Tripetide in the Gas-Phase: IR/UV Experiments, Ab Initio Quantum Chemical Calculations, and Molecular Dynamic Simulations. *Chem. - A Eur. J.* **2005**, *11*, 6803–6817.

(S15) Goerigk, L.; Grimme, S. A thorough benchmark of density functional methods for general main group thermochemistry, kinetics, and noncovalent interactions. *Phys. Chem. Chem. Phys.* **2011**, *13*, 6670–6688.

(S16) Grimme, S.; Steinmetz, M.; Korth, M. How to Compute Isomerization Energies of Organic Molecules with Quantum Chemical Methods. *J. Org. Chem.* **2007**, *72*, 2118–2126.

(S17) Curtiss, L. A.; Raghavachari, K.; Redfern, P. C.; Pople, J. A. Assessment of Gaussian-2 and density functional theories for the computation of enthalpies of formation. *J. Chem. Phys.* **1997**, *106*, 1063.

(S18) Goerigk, L.; Hansen, A.; Bauer, C.; Ehrlich, S.; Najibi, A.; Grimme, S. A look at the density functional theory zoo with the advanced GMTKN55 database for general main group thermochemistry, kinetics and noncovalent interactions. *Phys. Chem. Chem. Phys.* **2017**, *19*, 32184–32215.

(S19) Perdew, J. P.; Burke, K.; Ernzerhof, M. Generalized Gradient Approximation Made Simple. *Phys. Rev. Lett.* **1996**, *77*, 3865–3868.

(S20) Perdew, J. P.; Burke, K.; Ernzerhof, M. Erratum: Generalized gradient approximation made simple (Physical Review Letters (1996) 77 (3865)). *Phys. Rev. Lett.* **1997**, *78*, 1396.

(S21) Becke, A. D. Density-functional exchange-energy approximation with correct asymptotic behavior. *Phys. Rev. A* **1988**, *38*, 3098–3100.

(S22) Lee, C.; Yang, W.; Parr, R. G. Development of the Colle-Salvetti correlation-energy formula into a functional of the electron density. *Phys. Rev. B* **1988**, *37*, 785–789.

(S23) Tao, J.; Perdew, J. P.; Staroverov, V. N.; Scuseria, G. E. Climbing the Density Functional Ladder: Non-Empirical Meta-Generalized Gradient Approximation Designed for Molecules and Solids. *Phys. Rev. Lett.* **2003**, *91*, 146401.

(S24) Zhao, Y.; Truhlar, D. G. A new local density functional for main-group thermochemistry, transition metal bonding, thermochemical kinetics, and noncovalent interactions. *J. Chem. Phys.* **2006**, *125*, 194101.

(S25) Peverati, R.; Truhlar, D. G. M11-L: A local density functional that provides improved

accuracy for electronic structure calculations in chemistry and physics. *J. Phys. Chem. Lett.* **2012**, *3*, 117–124.

(S26) Becke, A. D. Density-functional thermochemistry. III. The role of exact exchange. *J. Chem. Phys.* **1993**, *98*, 5648.

(S27) Stephens, P. J.; Devlin, F. J.; Chabalowski, C. F.; Frisch, M. J. Ab Initio Calculation of Vibrational Absorption and Circular Dichroism Spectra Using Density Functional Force Fields. *J. Chem. Phys.* **1994**, *98*, 11623–11627.

(S28) Adamo, C.; Barone, V. Toward reliable density functional methods without adjustable parameters: The PBE0 model. *J. Chem. Phys.* **1999**, *110*, 6158.

(S29) Ernzerhof, M.; Scuseria, G. E. Assessment of the Perdew–Burke–Ernzerhof exchange-correlation functional. *J. Chem. Phys.* **1999**, *110*, 5029.

(S30) Becke, A. D. A new mixing of Hartree–Fock and local density-functional theories. *J. Chem. Phys.* **1993**, *98*, 1372.

(S31) Zhao, Y.; Truhlar, D. G. The M06 suite of density functionals for main group thermochemistry, thermochemical kinetics, noncovalent interactions, excited states, and transition elements: Two new functionals and systematic testing of four M06-class functionals and 12 other function. *Theor. Chem. Acc.* **2008**, *120*, 215–241.

(S32) Zhao, Y.; Truhlar, D. G. Density functional for spectroscopy: No long-range self-interaction error, good performance for Rydberg and charge-transfer states, and better performance on average than B3LYP for ground states. *J. Phys. Chem. A* **2006**, *110*, 13126–13130.

(S33) Lin, Y.-S.; Tsai, C.-W.; Li, G.-D.; Chai, J.-D. Long-range corrected hybrid meta-generalized-gradient approximations with dispersion corrections. *J. Chem. Phys.* **2012**, *136*, 154109.

(S34) Mardirossian, N.; Head-Gordon, M. ωB97X-V: A 10-parameter, range-separated hybrid, generalized gradient approximation density functional with nonlocal correlation, designed by a survival-of-the-fittest strategy. *Phys. Chem. Chem. Phys.* **2014**, *16*, 9904.

(S35) Mardirossian, N.; Head-Gordon, M. ωB97M-V: A combinatorially optimized, range-separated hybrid, meta-GGA density functional with VV10 nonlocal correlation. *J. Chem. Phys.* **2016**, *144*, 214110.

(S36) Peverati, R.; Truhlar, D. G. Improving the accuracy of hybrid meta-GGA density functionals by range separation. *J. Phys. Chem. Lett.* **2011**, *2*, 2810–2817.

(S37) Grimme, S.; Ehrlich, S.; Goerigk, L. Effect of the damping function in dispersion corrected density functional theory. *J. Comput. Chem.* **2011**, *32*, 1456–1465.

(S38) Vydrov, O. A.; Van Voorhis, T. Nonlocal van der Waals density functional: The simpler the better. *J. Chem. Phys.* **2010**, *133*, 244103.

(S39) Lee, T. J.; Taylor, P. R. A diagnostic for determining the quality of single-reference electron correlation methods. *Int. J. Quantum Chem.* **1989**, *36*, 199–207.

(S40) Jurečka, P.; Šponer, J.; Černý, J.; Hobza, P. Benchmark database of accurate (MP2 and CCSD(T) complete basis set limit) interaction energies of small model complexes, DNA base pairs, and amino acid pairs. *Phys. Chem. Chem. Phys.* **2006**, *8*, 1985–1993.

(S41) Řezáč, J.; Riley, K. E.; Hobza, P. S66: A well-balanced database of benchmark interaction energies relevant to biomolecular structures. *J. Chem. Theory Comput.* **2011**, *7*, 2427–2438.

(S42) Steinmann, S. N.; Corminboeuf, C. Exploring the Limits of Density Functional Approximations for Interaction Energies of Molecular Precursors to Organic Electronics. *J. Chem. Theory Comput.* **2012**, *8*, 4305–4316.

(S43) Liakos, D. G.; Sparta, M.; Kesharwani, M. K.; Martin, J. M. L.; Neese, F. Exploring the Accuracy Limits of Local Pair Natural Orbital Coupled-Cluster Theory. *J. Chem. Theory Comput.* **2015**, *11*, 1525–1539.

(S44) Liakos, D. G.; Guo, Y.; Neese, F. Comprehensive Benchmark Results for the Domain Based Local Pair Natural Orbital Coupled Cluster Method (DLPNO-CCSD(T)) for Closed- and Open-Shell Systems. *J. Phys. Chem. A* **2020**, *124*, 90–100.